ADVANCED MATERIALS
www.advmat.de

Inorganic Polymer Micropillar-Based Solution Shearing of Large-Area Organic Semiconductor Thin Films with Pillar-Size-Dependent Crystal Size

*Jin-Oh Kim, Jeong-Chan Lee, Min-Ji Kim, Hyunwoo Noh, Hye-In Yeom, Jong Beom Ko, Tae Hoon Lee, Sang-Hee Ko Park, Dong-Pyo Kim, and Steve Park**

It is demonstrated that the crystal size of small-molecule organic semiconductors can be controlled during solution shearing by tuning the shape and dimensions of the micropillars on the blade. Increasing the size and spacing of the rectangular pillars increases the crystal size, resulting in higher thin-film mobility. This phenomenon is attributed as the microstructure changing the degree and density of the meniscus line curvature, thereby controlling the nucleation process. The use of allylhybridpolycarbosilane (AHPCS), an inorganic polymer, is also demonstrated as the microstructured blade for solution shearing, which has high resistance to organic solvents, can easily be microstructured via molding, and is flexible and durable. Finally, it is shown that solution shearing can be performed on a curved surface using a curved blade. These demonstrations bring solution shearing closer to industrial applications and expand its applicability to various printed flexible electronics.

Solution processable small-molecule organic semiconductors are promising candidate as channel material in field-effect transistors for low-cost, large-area, lightweight, and flexible electronic applications.[1–5] Organic semiconductors can also be used with inorganic semiconductors for high-performance thin-film transistors.[6] The field-effect mobility of small-molecule organic semiconductor thin film is dependent on the crystallinity, crystal orientation, and molecular packing. Generally, larger crystals oriented along their fast transport axis yield higher field-effect mobility.[1,7] A variety of solution-based coating techniques have been developed over the past few decades to control the thin-film crystallization, such as nanostructured surface,[8] dip-coating,[9] zone casting,[10,11] brush-painting,[12] bar-coating,[13] slot-die coating,[14,15] pinned-growth,[16] hollow pen writing,[17] inkjet printing,[4,18] gravure printing,[19] and solution shearing.[4,5,7,11,14,20] Solution shearing, in particular, has been shown to generate highly crystalline and aligned organic crystals over a large area, making it a highly feasible technique for the fabrication of high-performance organic field-effect transistors.[3,7,21] Recently, solution shearing technique was further improved by using microstructured silicon blade, which disrupts laminar flow and enhances mass transport, resulting in thin film with a reduced density of dendrites and voids (i.e., regions absent of thin-film material).[3] Lately, it was also shown that surface modification of the microstructured blade influences crystal growth.[22] Despite the demonstration of high-quality thin films, these studies have not fully controlled both crystal size and the density of voids simultaneously. Furthermore, microstructured blades are currently being fabricated with silicon, which have key limitations such as high cost and difficulty in processing (as it requires photolithography and multiple etching steps), and brittleness that makes it easily breakable during solution shearing operation. These features render microstructured silicon blade difficult to be implemented into industrial setting where low cost and durability are of great importance. Elastomers such as poly(dimethylsiloxane) (PDMS), which can easily be microstructured by casting onto a mold, can be used; however, such elastomers are generally susceptible to organic solvents (i.e., swelling), significantly limiting their use in solution shearing. Therefore, adopting a new material is needed that is resistant to organic solvents, low cost, easily processable, and mechanically durable.

J.-O. Kim, J.-C. Lee, M.-J. Kim, Prof. S. Park
Organic and Nano Electronics Laboratory
Department of Materials Science and Engineering
Korea Advanced Institute of Science and Technology (KAIST)
Yuseong-gu, Daejeon 34141, Republic of Korea
E-mail: stevepark@kaist.ac.kr

H. Noh
Department of Mechanical Engineering
Pohang University of Science and Technology (POSTECH)
Pohang, Gyeongbuk 37673, Republic of Korea

The ORCID identification number(s) for the author(s) of this article can be found under https://doi.org/10.1002/adma.201800647.

DOI: 10.1002/adma.201800647

H.-I. Yeom, J. B. Ko, Prof. S.-H. Ko Park
Department of Materials Science and Engineering
Korea Advanced Institute of Science and Technology (KAIST)
Yuseong-gu, Daejeon 34141, Republic of Korea

Prof. T. H. Lee
Department of Electrical Engineering
Kwangwoon University
Nowon-gu, Seoul 01897, Republic of Korea

Prof. D.-P. Kim
Center for Intelligent Microprocess of Pharmaceutical Synthesis (CIMPS)
Department of Chemical Engineering
Pohang University of Science and Technology (POSTECH)
Pohang, Gyeongbuk 37673, Republic of Korea

Herein, we introduce the use of a silicon-based inorganic polymer, allylhybridpolycarbosilane (AHPCS), as microstructured blade for solution shearing. AHPCS can easily be microstructured via conventional molding technique, has high mechanical durability and solvent resistance.[23,24] Moreover, we demonstrate, for the first time, that solely by tuning the shape and dimension of the microstructure, we can control the size of 6,13-bis(triisopropylsilylethynyl)pentacene (TIPS-pentacene) crystals, thereby improving the field-effect mobility of the thin film. We attribute this phenomenon to different microstructures inducing varying the degree and density of curvatures in the meniscus line, through which nucleation can be regulated. Hence, the control of nucleation and, therefore, the crystal size via tuning the microstructured blade pattern add another key parameter that can be utilized to tune the properties of organic thin films.

Figure 1a shows the chemical structure of AHPCS resin. Figure 1b is a schematic depiction of the microstructured AHPCS shearing blade fabrication process. AHPCS resin is placed on top of a substrate (glass or PDMS), followed by the placement of PDMS mold on top. Subsequent UV curing induces cross-linking and hardens AHPCS.[23,25,26] The PDMS can easily be lifted off the cross-linked AHPCS surface. As with silicon, the surface of AHPCS can be easily modified to tune its wettability. For instance, after hydrolysis reaction in NaOH solution (which generates hydroxyl groups on the surface of AHPCS),[26,27] the water contact angle of AHPCS changes from 92° to 12° (Figure 1c,d).[27] To make the surface hydrophobic, the hydroxyl groups were reacted with trichloro-(1*H*,1*H*,2*H*,2*H*-perfluorooctyl)silane self-assembled monolayer, which changed the water contact angle of AHPCS micropillar surface from 12° to 145° (Figure 1e).[28] Being able to control the wettability of blade surface is an important feature in solution shearing as it can change the thin-film morphology.[7,22]

Figure S1 (Supporting Information) are optical images of the microstructured AHPCS blade after immersion in various organic solvents, which shows no swelling or damage. Solvent resistance of AHPCS has also been studied previously.[23,24] This is in contrast to PDMS, which has previously been shown to swell in various organic solvents.[29] Furthermore, unlike silicon, AHPCS is flexible, retaining the shape of the microstructure even after 20 bending cycles down to 6 mm radius of curvature (Figure S2, Supporting Information). We have also tested the elasticity of the pillars under repeated application and release of 50 kPa of compressive stress (20 cycles), where we have observed the pillars retaining their shape (Figure S3, Supporting Information). These features together render AHPCS advantageous over PDMS and silicon.

Figure 2a is the schematic diagram of solution shearing process using microstructured AHPCS blade. In solution shearing, organic solution is sandwiched between a blade and a substrate, where meniscus forms at the edge of the blade. Since the liquid layer is the thinnest at the edge of the meniscus (i.e., meniscus line), this region has a relatively high solvent evaporation rate. This causes supersaturation along the meniscus line, and consequently, nucleation and crystal growth are induced. By controlling the shearing rate and the substrate temperature, the growing crystal can propagate along with the moving blade across the substrate. To control the nucleation during solution shearing, wetting and dewetting regions are generally patterned on the substrate to locally generate a sharp curvature in the meniscus line. This locally accelerates solvent evaporation rate and tunnels in solute into a narrow region, inducing nucleation.[3,21,30] Controlling nucleation is highly important as

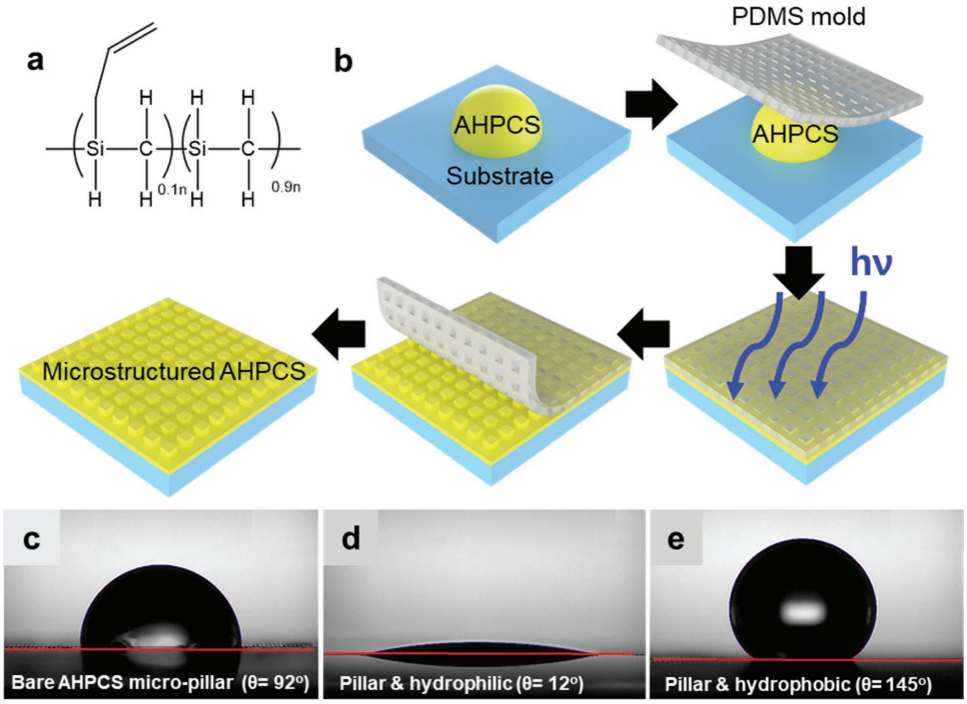

Figure 1. a) The chemical structure of AHPCS resin. b) Schematic illustration of the fabrication process of microstructured AHPCS shearing blade. Optical images of water contact angle with: c) the bare, d) hydrophilic, and e) hydrophobic AHPCS micropillar surface.

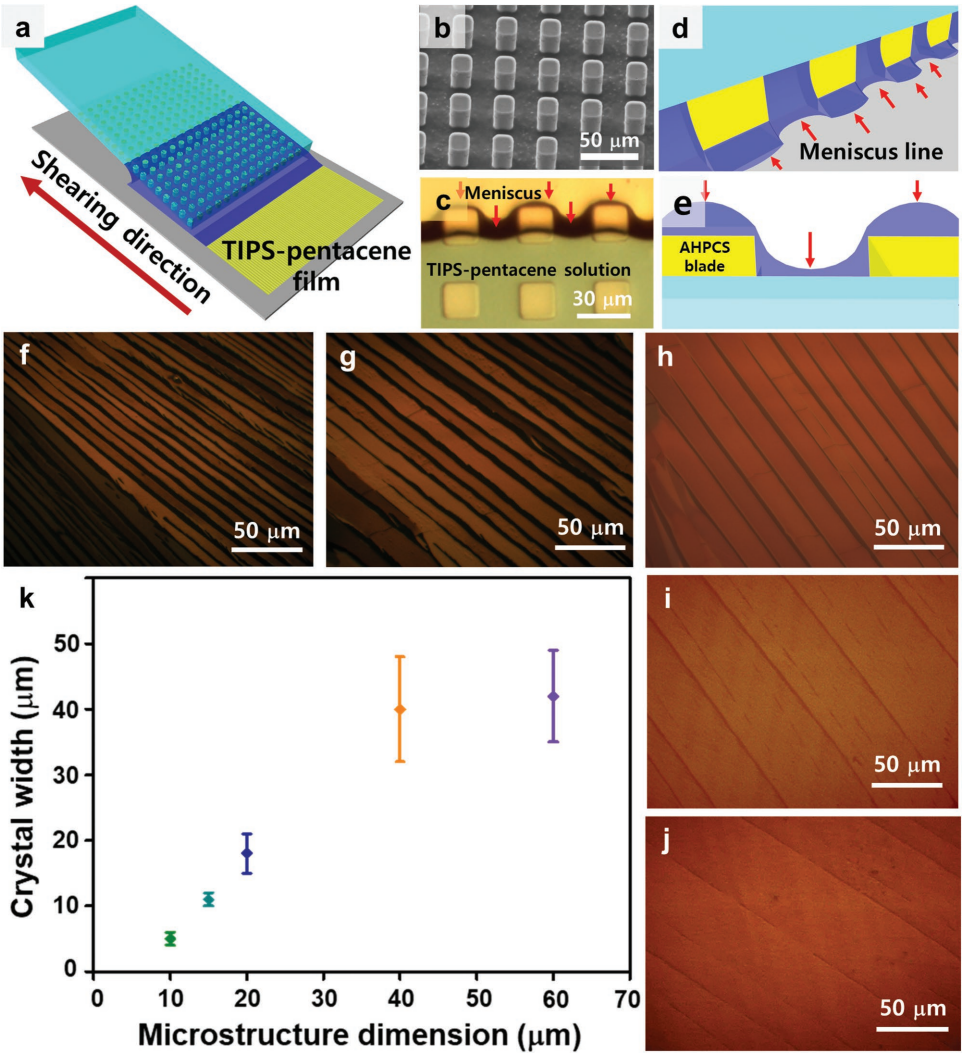

Figure 2. a) Schematic illustration of the overall solution shearing process using microstructured AHPCS blade. b) Scanning electron microscopy (SEM) image of AHPCS shearing blade with a microstructure dimension of 20 μm. c) The top view image of the meniscus line formed on the substrate. d,e) Schematic of the curvature of the meniscus line formed between the AHPCS blade and the substrate. The red arrows indicate the regions with the highest curvature in the meniscus line. f–j) Cross-polarized optical microscopy images of TIPS-pentacene thin films solution-sheared using AHPCS shearing blade with microstructure dimensions of 10 μm (f), 15 μm (g), 20 μm (h), 40 μm (i), and 60 μm (j). k) Average TIPS-pentacene crystal width versus the microstructure dimension of the AHPCS shearing blade. The vertical bars indicate standard deviation.

it can be used to tune the crystal size, and therefore the property of the thin film. However, the aforementioned technique complicates the fabrication process as it requires patterning of multiple types of self-assembled monolayers.

Figure 2b shows microstructured shearing blade with rectangular-shaped pillars arranged as square Bravais lattice. We fabricated five different microstructured blades of this type with pillar width, edge-to-edge spacing, and pillar height all proportionally scaled to 10, 15, 20, 40, and 60 μm, respectively. From this point forward, we will refer to this scale as "microstructure dimensions." Figure 2f–j shows optical images of solution-sheared TIPS-pentacene (2 mg mL^{-1} in toluene at 0.5 mm s^{-1}, a substrate temperature of 85 °C) with blades of the five aforementioned microstructure dimensions. Figure 2k shows that the average crystal width increases with increasing microstructure dimension of the shearing blade up to 40 μm, after which crystal width starts to saturate. Such an increasing trend can be attributed to the changing density of sharp curvature regions in the meniscus line with different microstructure dimensions. We have taken an optical image of the meniscus line as seen in Figure 2c (Figure S4, Supporting Information), where we see that in the region absent of the rectangular pillar, the meniscus line is receded. On the other hand, in the region where the rectangular pillar is present, the meniscus line is pinned and is therefore protruding outward. This phenomenon is schematically depicted in Figure 2d,e. Such a difference in wetting properties of the solution can be attributed to the difference in surface energy balance of the substrate–liquid–air–blade interfaces.[31] Since the curvature of the meniscus line is highest at the center of the pillars and in the center between the pillars (as indicated by arrows in Figure 2c–e), there is a relatively higher probability that nucleation will occur in these regions.

With decreasing pillar width and spacing, the density of these high curvature regions increases, leading to denser nucleation and thus small crystal widths. It is important to note that controlling the meniscus line curvature does not completely prevent nucleation from occurring elsewhere. Nucleation is by nature a stochastic process, but we are increasing the likelihood of nucleation in certain regions through accelerating the solvent evaporation and supersaturation process. We hypothesize that beyond the microstructure dimension of 40 µm, the density of the high curvature region is too low, and the stochastic nature overtakes the nucleation process.

We have also tested circular, V-shaped, and Λ-shaped pillars of various dimensions (width, spacing, and height all proportionally scaled). Interestingly, we did not observe any dependence of crystal width on the different circular and V-shaped microstructure dimensions (Figures S5 and S6, Supporting Information). From the observation of meniscus lines, the circular and the V-shaped pillars did not effectively generate sharp curvatures in the meniscus line, especially in the regions absent of the pillars. Hence, the nucleation control was likely not so effective. For the Λ-shaped pillars, the crystal width increased slightly with increasing pillar dimensions (Figure S7, Supporting Information). The meniscus was pinned at the peaks of the pillars inducing local sharp curvatures; however, in between the pillars, the curvature was not as sharp as the rectangular pillars. Hence, although nucleation likely occurred locally at the pinned points, the suppression of nucleation elsewhere was weak, resulting in only slightly increasing crystal width with pillar dimensions. Therefore, among the pillar shapes we have tested, the rectangular pillars most effectively controlled crystal width due to its ability to generate sharp angles in the meniscus line, which facilitate nucleation control.

Using thin films solution-sheared with rectangular pillars of various dimensions, thin-film transistors were fabricated. Heavily doped silicon and 300 nm thick silicon oxide were used as the bottom gate and gate dielectric layer, respectively. Top source/drain contacts of 100 nm thick Au were thermally evaporated on top of the organic film. The channel length and channel width of the devices were 40 and 400 µm, respectively. Figures S8–S10 in the Supporting Information are

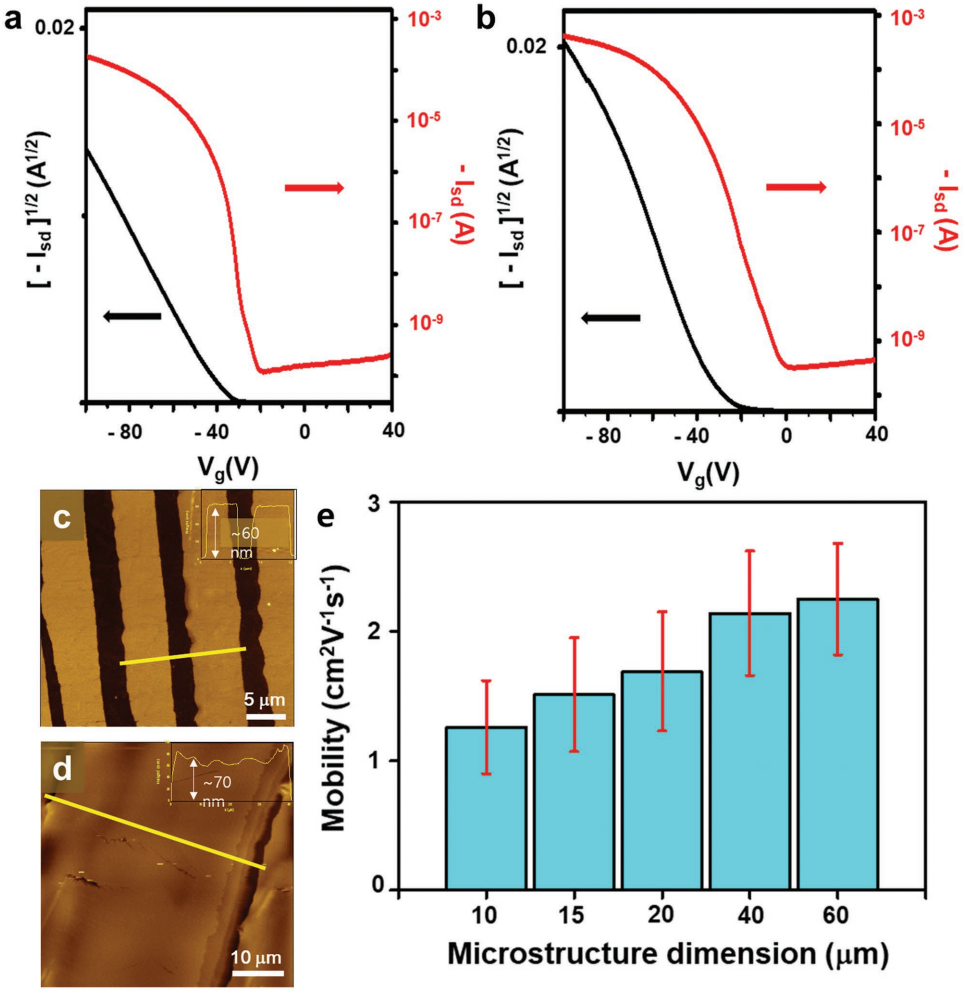

Figure 3. a,b) Representative transfer characteristics of field-effect transistor fabricated using AHPCS shearing blade with microstructure dimensions of 10 and 60 µm, respectively. The source–drain voltage was –100 V. c,d) AFM images and height profiles of thin films sheared with blade microstructure dimensions of 10 and 60 µm, respectively. e) Comparison of average field-effect mobility of field-effect transistors solution-sheared with microstructure dimensions of 10, 15, 20, 40, and 60 µm. The vertical bars represent standard deviation.

histograms of mobility, threshold voltage, and on/off ratios for the devices made with different microstructure dimensions. For each microstructure dimension, 30 devices were measured. **Figure 3**a,b shows representative transfer curves for devices fabricated with shearing blade microstructure dimensions of 10 and 60 µm, respectively. Figure S11 in the Supporting Information shows the typical gate leakage current of our devices, which was smaller than the source–drain current. Figure 3c,d are close-up atomic force microscopy (AFM) images and height profiles of thin films made with shearing blade microstructure dimensions of 10 and 60 µm, respectively. The AFM images show relatively smooth crystal surface with a thickness of 60–70 nm. Figure 3e is a plot of average field-effect mobility of 30 devices versus microstructure dimensions, which shows increasing trend in field-effect mobility with increasing microstructure dimensions. With the 60 µm microstructure dimensions, an average mobility of 2.26 $cm^2\ V^{-1}\ s^{-1}$ and a maximum mobility of 3.56 $cm^2\ V^{-1}\ s^{-1}$ were obtained. The increasing trend in mobility can first be attributed to the lower density of voids (i.e., regions absent of TIPS-pentacene) for the film composed of larger crystals (i.e., field-effect mobility was calculated using the width of the electrodes). Furthermore, charge scattering has been shown to occur at the edge of the crystals;[32] therefore, films with larger crystal widths (i.e., lower density of edges) are expected to have higher mobility.

Finally, we demonstrate that unlike a silicon-based shearing blade, AHPCS-based shearing blade can be made into a curved shape, through which we can coat thin film on a curved surface (**Figure 4**a). This technique can be used to coat films directly on variety of nonplanar surfaces, greatly expanding the applicability of solution shearing. Furthermore, this technique can be useful for fabricating devices with small radius of curvature, where some materials can undergo cracking if bent from a flat state. To fabricate a curved shearing blade, we have used PDMS as the substrate; thereafter, we attached the PDMS/microstructured AHPCS onto a secondary curved PDMS substrate (detailed in the Supporting Information). Figure 4b is an optical image of a curved shearing blade. We attached a flexible device (polyimide as the substrate, Mo as the gate electrode, and aluminum oxide as the gate dielectric) onto a glass vial with the same curvature as the shearing blade (Figure 4c), and solution-sheared TIPS-pentacene onto the device. Figure 4d is the cross-polarized microscopy image of the TIPS-pentacene thin film. Subsequently, we evaporated source and drain electrodes to complete the device (Figure 4e). Figure 4f and Figure S12 in the Supporting Information show typical transfer characteristics of the curved devices. The field-effect mobility ranged between 0.1 and 0.3 $cm^2\ V^{-1}\ s^{-1}$, which were lower than the devices fabricated on silicon substrates. This can be attributed to the

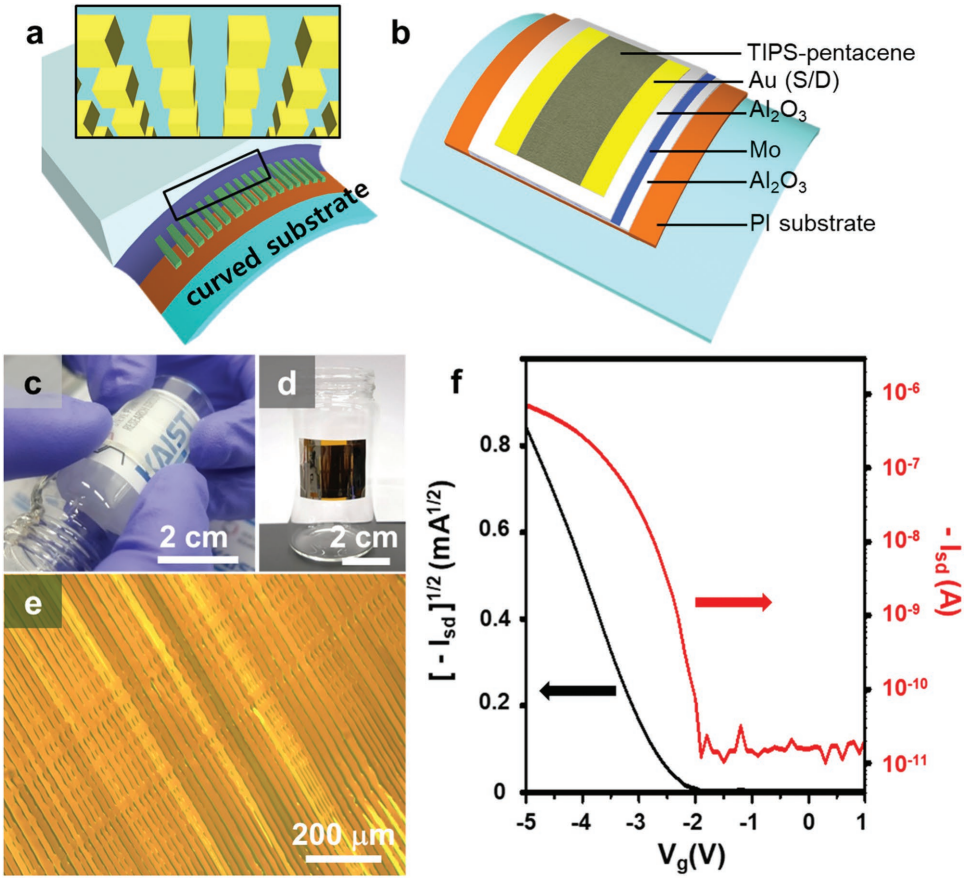

Figure 4. a) Schematic illustration of the solution shearing process on a curved surface using curved AHPCS shearing blade and b) optical image of a curved microstructured blade. c) Optical image of a curved device on a glass vial. d) Cross-polarized optical microscopy image of TIPS-pentacene thin film solution-sheared on a curved surface using a curved shearing blade. e) Schematic of a curved field-effect transistor. f) Transfer characteristics of a curved field-effect transistor. The source–drain voltage was −2 V.

difference in the charge trap state in the dielectric layer and the dielectric–semiconductor interface.[33] Further investigation is needed to improve the device performance of the curved devices, and this is the topic of our future work.

In summary, we demonstrate the application of a novel material, AHPCS, for microstructured blade in solution shearing. For AHPCS, microstructure can easily be fabricated using the simple soft-lithography process. In addition, AHPCS is highly resistant to various organic solvents and has high mechanical flexibility and durability, making it advantageous over silicon and elastomers such as PDMS. Furthermore, we have fabricated rectangular pillars arranged as square Bravais lattice, where we observed the average crystal width increase with the width and spacing of the pillars. We attribute this phenomenon to the difference in the density of local high curvatures generated in the meniscus line, at which solvent evaporation rate is accelerated and nucleation is hence induced. Increasing crystal width correspondingly resulted in increasing field-effect mobility. Such a control of crystal size by manipulating the shape and size of the microstructure on the shearing blade adds another useful parameter that can be utilized to tune the property of thin films. Lastly, we demonstrate that thin film can be solution-sheared on a curved surface, opening up a wide variety of new applications.

Experimental Section

Experimental materials and methods as well as additional results are part of the Supporting Information.

Supporting Information

Supporting Information is available from the Wiley Online Library or from the author.

Acknowledgements

J.-O.K. and J.-C.L. contributed equally to this work. This work was supported by National Research Foundation of Korea (NRF) grant funded by the Korea government (No. 2017047921, 10070075, and No. 2016R1C1B1014935) and support by Nano Material Technology Development Program through the National Research Foundation of Korea (NRF) funded by the Ministry of Science, ICT and Future Planning (2009-0082580).

Conflict of Interest

The authors declare no conflict of interest.

Keywords

inorganic polymers, microstructuring, soft lithography, solution shearing, TIPS-pentacene

Received: January 29, 2018
Revised: March 26, 2018
Published online: May 28, 2018

[1] B. Kang, W. H. Lee, K. Cho, *ACS Appl. Mater. Interfaces* **2013**, *5*, 2302.
[2] Y. Yan, L. B. Huang, Y. Zhou, S. T. Han, L. Zhou, J. Zhuang, Z. X. Xu, V. A. Roy, *Sci. Rep.* **2015**, *5*, 15770.
[3] Y. Diao, B. C. Tee, G. Giri, J. Xu, D. H. Kim, H. A. Becerril, R. M. Stoltenberg, T. H. Lee, G. Xue, S. C. Mannsfeld, Z. Bao, *Nat. Mater.* **2013**, *12*, 665.
[4] H. Minemawari, T. Yamada, H. Matsui, J. Tsutsumi, S. Haas, R. Chiba, R. Kumai, T. Hasegawa, *Nature* **2011**, *475*, 364.
[5] A. Russo, B. Y. Ahn, J. J. Adams, E. B. Duoss, J. T. Bernhard, J. A. Lewis, *Adv. Mater.* **2011**, *23*, 3426.
[6] a) G. Kwon, K. Kim, B. D. Choi, J. Roh, C. Lee, Y. Y. Noh, S. Seo, M. G. Kim, C. Kim, *Adv. Mater.* **2017**, *29*, 1607055; b) L. Wang, M. H. Yoon, G. Lu, Y. Yang, A. Facchetti, T. J. Marks, *Nat. Mater.* **2006**, *5*, 893.
[7] G. Giri, E. Verploegen, S. C. Mannsfeld, S. Atahan-Evrenk, D. H. Kim, S. Y. Lee, H. A. Becerril, A. Aspuru-Guzik, M. F. Toney, Z. Bao, *Nature* **2011**, *480*, 504.
[8] D. E. Johnston, K. G. Yager, H. Hlaing, X. Lu, B. M. Ocko, C. T. Black, *ACS Nano* **2014**, *8*, 243.
[9] a) C. W. Sele, B. K. C. Kjellander, B. Niesen, M. J. Thornton, J. van der Putten, K. Myny, H. J. Wondergem, A. Moser, R. Resel, A. van Breemen, N. van Aerle, P. Heremans, J. E. Anthony, G. H. Gelinck, *Adv. Mater.* **2009**, *21*, 4926; b) H. N. Tsao, D. Cho, J. W. Andreasen, A. Rouhanipour, D. W. Breiby, W. Pisula, K. Müllen, *Adv. Mater.* **2009**, *21*, 209; c) M. Li, C. An, W. Pisula, K. Mullen, *Small* **2014**, *10*, 1926; d) H. Zhao, Z. Wang, G. Dong, L. Duan, *Phys. Chem. Chem. Phys.* **2015**, *17*, 6274.
[10] a) M. Mas-Torrent, S. Masirek, P. Hadley, N. Crivillers, N. S. Oxtoby, P. Reuter, J. Veciana, C. Rovira, A. Tracz, *Org. Electron.* **2008**, *9*, 143; b) D. T. James, J. M. Frost, J. Wade, J. Nelson, J.-S. Kim, *ACS Nano* **2013**, *7*, 7983; c) C. M. Duffy, J. W. Andreasen, D. W. Breiby, M. M. Nielsen, M. Ando, T. Minakata, H. Sirringhaus, *Chem. Mater.* **2008**, *20*, 7252.
[11] W. Pisula, A. Menon, M. Stepputat, I. Lieberwirth, U. Kolb, A. Tracz, H. Sirringhaus, T. Pakula, K. Müllen, *Adv. Mater.* **2005**, *17*, 684.
[12] Z. Qi, F. Zhang, C.-a. Di, J. Wang, D. Zhu, *J. Mater. Chem. C* **2013**, *1*, 3072.
[13] D. Khim, H. Han, K. J. Baeg, J. Kim, S. W. Kwak, D. Y. Kim, Y. Y. Noh, *Adv. Mater.* **2013**, *25*, 4302.
[14] J. Chang, C. Chi, J. Zhang, J. Wu, *Adv. Mater.* **2013**, *25*, 6442.
[15] A. K. Kyaw, L. S. Lay, G. W. Peng, J. Changyun, Z. Jie, *Chem. Commun.* **2016**, *52*, 358.
[16] a) H. Li, B. C. K. Tee, J. J. Cha, Y. Cui, J. W. Chung, S. Y. Lee, Z. Bao, *J. Am. Chem. Soc.* **2012**, *134*, 2760; b) S. Liu, J.-K. Wu, C.-C. Fan, G.-B. Xue, H.-Z. Chen, H. L. Xin, H.-Y. Li, *Sci. Bull.* **2015**, *60*, 1122.
[17] a) Y. Wang, L. Chen, Q. Wang, H. Sun, X. Wang, Z. Hu, Y. Li, Y. Shi, *Org. Electron.* **2014**, *15*, 2234; b) R. L. Headrick, S. Wo, F. Sansoz, J. E. Anthony, *Appl. Phys. Lett.* **2008**, *92*, 063302; c) S. Wo, R. L. Headrick, J. E. Anthony, *J. Appl. Phys.* **2012**, *111*, 073716.
[18] J. A. Lim, W. H. Lee, H. S. Lee, J. H. Lee, Y. D. Park, K. Cho, *Adv. Funct. Mater.* **2008**, *18*, 229.
[19] a) A. de la Fuente Vornbrock, D. Sung, H. Kang, R. Kitsomboonloha, V. Subramanian, *Org. Electron.* **2010**, *11*, 2037; b) M. M. Voigt, A. Guite, D.-Y. Chung, R. U. A. Khan, A. J. Campbell, D. D. C. Bradley, F. Meng, J. H. G. Steinke, S. Tierney, I. McCulloch, H. Penxten, L. Lutsen, O. Douheret, J. Manca, U. Brokmann, K. Sönnichsen, D. Hülsenberg, W. Bock, C. Barron, N. Blanckaert, S. Springer, J. Grupp, A. Mosley, *Adv. Funct. Mater.* **2010**, *20*, 239; c) M. Hambsch, K. Reuter, M. Stanel, G. Schmidt, H. Kempa, U. Fügmann, U. Hahn, A. C. Hübler, *Mater. Sci. Eng., B* **2010**, *170*, 93.
[20] a) L. Qiu, J. A. Lim, X. Wang, W. H. Lee, M. Hwang, K. Cho, *Adv. Mater.* **2008**, *20*, 1141; b) J. Lim, W. Lee, D. Kwak, K. Cho, *Langmuir* **2009**, *25*, 5404.

[21] a) G. Giri, S. Park, M. Vosgueritchian, M. M. Shulaker, Z. Bao, *Adv. Mater.* **2014**, *26*, 487; b) S. Park, G. Giri, L. Shaw, G. Pitner, J. Ha, J. H. Koo, X. Gu, J. Park, T. H. Lee, J. H. Nam, Y. Hong, Z. Bao, *Proc. Natl. Acad. Sci. USA* **2015**, *112*, 5561.
[22] C. Xiao, X. Kan, C. Liu, W. Jiang, G. Zhao, Q. Zhao, L. Zhang, W. Hu, Z. Wang, L. Jiang, *J. Mater. Chem. C* **2017**, *5*, 2702.
[23] Z. Xiao, A. Wang, D.-P. Kim, *J. Mater. Chem.* **2010**, *20*, 2853.
[24] S. Park, D. H. Lee, H. I. Ryoo, T. W. Lim, D. Y. Yang, D. P. Kim, *Chem. Commun.* **2009**, 4880.
[25] a) Z. Xiao, A. Wang, J. Perumal, D. P. Kim, *Adv. Funct. Mater.* **2010**, *20*, 1473; b) Z. Xiao, Y. Zhao, A. Wang, J. Perumal, D. P. Kim, *Lab Chip* **2011**, *11*, 57.
[26] H. Noh, J. O. Kim, D. H. Kim, H. S. Park, Y. H. Hwang, M. H. Kim, D. P. Kim, *Adv. Mater. Interfaces* **2016**, *3*, 1600507.
[27] M. Li, D. P. Kim, *Lab Chip* **2011**, *11*, 1126.
[28] D.-H. Ko, W. Ren, J.-O. Kim, J. Wang, H. Wang, S. Sharma, M. Faustini, D.-P. Kim, *ACS Nano* **2016**, *10*, 1156.
[29] J. N. Lee, C. Park, G. M. Whitesides, *Anal. Chem.* **2003**, *75*, 6544.
[30] Y. Wu, J. Feng, B. Su, L. Jiang, *Adv. Mater.* **2016**, *28*, 2266.
[31] a) A. A. Saha, S. K. Mitra, M. Tweedie, S. Roy, J. McLaughlin, *Microfluid. Nanofluid.* **2009**, *7*, 451; b) C. Semprebon, P. Forsberg, C. Priest, M. Brinkmann, *Soft Matter* **2014**, *10*, 5739.
[32] a) C. Liu, K. Huang, W.-T. Park, M. Li, T. Yang, X. Liu, L. Liang, T. Minari, Y.-Y. Noh, *Mater. Horiz.* **2017**, *4*, 608; b) D. Venkateshvaran, M. Nikolka, A. Sadhanala, V. Lemaur, M. Zelazny, M. Kepa, M. Hurhangee, A. J. Kronemeijer, V. Pecunia, I. Nasrallah, I. Romanov, K. Broch, I. McCulloch, D. Emin, Y. Olivier, J. Cornil, D. Beljonne, H. Sirringhaus, *Nature* **2014**, *515*, 384.
[33] a) J. Robertson, *Rep. Prog. Phys.* **2006**, *69*, 327; b) A. L. Deman, J. Tardy, *Mater. Sci. Eng., C* **2006**, *26*, 421.